Annals of Solid and Structural Mechanics (2019) 11:11–24
https://doi.org/10.1007/s12356-019-00053-4

ORIGINAL ARTICLE

2D dynamic and earthquake response analysis of base isolation systems using a convex optimization framework

Nicholas D. Oliveto[1] · Anastasia Athanasiou[2]

Received: 5 September 2018 / Accepted: 9 October 2019 / Published online: 23 October 2019

Abstract

A formulation is presented for the 2D dynamic analysis and earthquake response simulation of base isolation systems. The approach is force-based and consists of casting the computation in each time increment as a convex optimization problem. Interaction between the two horizontal components of response is considered in an elegant and simple way through yield functions appearing as constraints of the optimization problem. Numerical examples are carried out to illustrate the approach. These comprise bidirectional shearing of a high damping rubber bearing and earthquake simulations of a real-world base isolation system.

Keywords Nonlinear dynamics · Seismic isolation · Convex optimization

1 Introduction

Seismic isolation is nowadays widely used across the world as one of the most effective techniques for the protection of buildings and bridges from earthquakes. By introducing a layer of low lateral stiffness devices between the structure and the foundation, base isolation has the effect of reducing the earthquake-induced forces in the superstructure. The seismic devices that are most commonly adopted are basically of two types, (1) rubber bearings and (2) sliding isolators. Extensive experimental and analytical work has been carried out to investigate and simulate the behavior of these devices. For a comprehensive review of the literature on modelling and analysis of rubber bearings and sliding isolators, the reader is referred to recent work by Markou et al. [1] and Calvi and Calvi [2]. With a few exceptions [3–6], existing models are generally unidirectional [7–11] and, in most cases, difficult to extend to general bidirectional loading. However, experiments on different types of rubber isolators [3, 12, 13] have shown that coupling effects between orthogonal components of response should be considered when the bearings are subjected to bidirectional loading. The aim of the present paper is to develop a simple, accurate and robust formulation for the 2D nonlinear dynamic analysis of base isolation systems, and to provide a basis for the dynamic identification of these systems under any kind of environmental and engineered excitation, including earthquake ground motions and release tests. To this end, a biaxial bilinear model is used in this work to characterize the behavior of the isolators. Nonlinear structural mechanics problems in general, as those related to dynamic analysis of base-isolated structures, are usually analyzed using displacement-based strategies where time integration methods, generally coupled with an iterative procedure of the Newton type, are used to solve the nonlinear equilibrium equations [14–16]. A different approach is taken in this paper where the computation in each time increment is cast as a mathematical program. Classic examples of mathematical programming include convex optimization, linear complementarity problems, and conic optimization (or complementarity over cones) [17–19]. By formulating the incremental state update problem as a mathematical program, the following attractive features may be exploited: (1) algorithms and solvers exist that can be invoked for the solution of a particular mathematical program, (2) these algorithms have excellent convergence characteristics, (3) questions about whether the problem is well-posed, and about the existence and uniqueness of solutions may be explored and answered. The use of mathematical programs for nonlinear structural

✉ Nicholas D. Oliveto
noliveto@buffalo.edu

1 Department of Civil and Architectural Engineering, University of Catania, Catania, Italy

2 Department of Building, Civil and Environmental Engineering, Concordia University, Montreal, Canada

analysis was first proposed in the seventies by Maier et al. [20, 21]. More recently, Sivaselvan et al. [22] developed an optimization-based algorithm for collapse simulation of large-scale structural systems. Sivaselvan [23], later developed a formulation for the nonlinear dynamic analysis of framed structures with softening plastic hinges based on casting the incremental state update as a complementarity problem. Oliveto and Sivaselvan [24] then extended such formulation to the dynamic analysis of tensegrity structures. In this work, the incremental state update problem is formulated as a convex minimization problem. The constraints of the optimization problem are yield functions representing interaction between the two horizontal components of isolator response. The organization of the paper is as follows. The equations of motion of a base-isolated building and the constitutive behavior used to model the isolators are illustrated in Sect. 2. Next, in Sect. 3, the governing equations of the spatially discretized base isolation system are discretized in time and their solution is set up as a convex optimization problem. Finally, in Sect. 4, a real-world base isolation system is introduced and static and dynamic numerical simulations are carried out to illustrate the proposed approach.

2 Modeling of base isolation systems

The equations of motion of a base isolation system may be written as:

$$\mathbf{M}\dot{\mathbf{v}}_0 + \mathbf{C}\mathbf{v}_0 + \mathbf{H}^T\mathbf{F} = \mathbf{P} \tag{1}$$

where $\mathbf{F} \in \mathbb{R}^{2N}$ is the vector of shear forces in the isolators, N being the total number of isolators in the system, $\mathbf{v}_0 \in \mathbb{R}^{N_{DOF}}$ is the vector of velocities at the N_{DOF} degrees of freedom of the base isolation system, $\mathbf{H} \in \mathbb{R}^{2N\times N_{DOF}}$ is the transformation matrix that relates displacements, velocities, and accelerations ($\mathbf{u}$, $\mathbf{v}$, and $\mathbf{a}$) of the isolators, to $\mathbf{u}_0$, $\mathbf{v}_0$, and $\mathbf{a}_0$, the global N_{DOF} degrees of freedom of the system, $\mathbf{M} \in \mathbb{R}^{N_{DOF}\times N_{DOF}}$ is the mass matrix, $\mathbf{C} \in \mathbb{R}^{N_{DOF}\times N_{DOF}}$ is the damping matrix, and $\mathbf{P} \in \mathbb{R}^{N_{DOF}}$ is the vector of external forces.

The constitutive behavior of the isolators is herein formulated using the *Generalized Standard Material Framework* [25, 26]. Representations of this kind apply to any dynamic model of a structural system, or component, whose constitutive behavior can be derived from stored energy and dissipation functions [22]. In this work, the constitutive equations are described in terms of biaxial shear forces in the isolators. For a generic isolator, i, we have $\mathbf{F}_i = (F_{i1}, F_{i2})^T$. In the following subsections, we characterize the constitutive behavior of high damping rubber bearings (HDRBs) and low friction sliding bearings (LFSBs). A hybrid base isolation system (HBIS) comprising these two types of isolators will be the subject of a series of numerical simulations presented in a later section.

2.1 High damping rubber bearings

The shear behavior of the HDRBs is herein characterized by extending to two dimensions the bilinear model with kinematic hardening shown in Fig. 1. This kind of a model, tuned according to the maximum strain amplitude of interest, is widely adopted in practice for the analysis and design of HDRBs [27]. Using the generalized material formalism, we define the following form of complementary stored energy:

$$\psi^c(\mathbf{F}_i, \boldsymbol{\zeta}_i) = \frac{1}{2}\mathbf{F}_i^T\mathbf{A}_{Ri}\mathbf{F}_i + \frac{1}{2}\boldsymbol{\zeta}_i^T\mathbf{A}_{hi}\boldsymbol{\zeta}_i \tag{2}$$

where $\mathbf{A}_{Ri} = \mathrm{diag}(1/k_0, 1/k_0)$ is the matrix of elastic compliances, $\mathbf{A}_{hi} = \mathrm{diag}(1/k_h, 1/k_h)$ is the matrix of compliances related to hardening, and $\boldsymbol{\zeta}_i$ denotes the internal variables for plasticity. Moreover, the following complementary dissipation function is used:

$$\phi^c(\mathbf{F}_i, \boldsymbol{\zeta}_i) = \chi_E(\mathbf{F}_i, \boldsymbol{\zeta}_i) \tag{3}$$

where χ_E is the indicator function of the elastic region given by the convex set

$$E = \left\{ (\mathbf{F}_i, \boldsymbol{\zeta}_i) \middle| \varphi(\mathbf{F}_i, \boldsymbol{\zeta}_i) < 0 \right\} \tag{4}$$

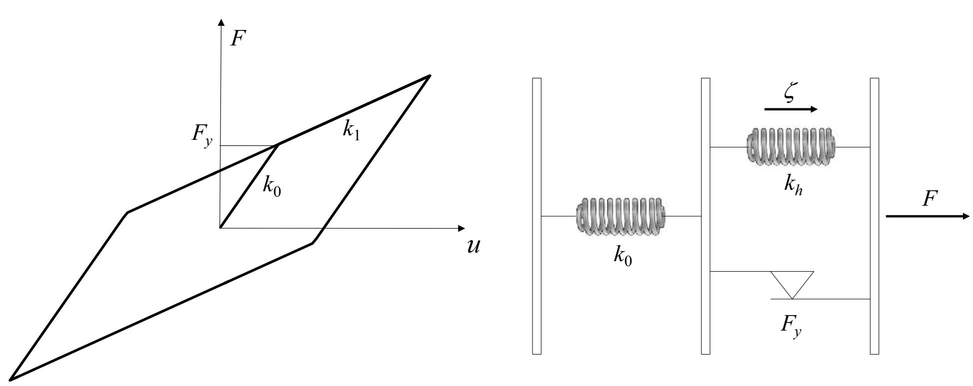

Fig. 1 1D constitutive model for HDRBs

and φ is a yield function. The indicator [28, 29] function, χ_E, is defined as

$$\chi_E(\mathbf{x}) = \begin{cases} 0 & \text{if} \quad \mathbf{x} \in E \\ \infty & \text{otherwise} \end{cases} \tag{5}$$

In the case of one-dimensional kinematic hardening, as shown in Fig. 1, complementary stored energy, ψ^c, and yield function, φ, are given by

$$\psi^c(F,\zeta) = \frac{1}{2}\frac{F^2}{k_0} + \frac{1}{2}\frac{\zeta^2}{k_h} \qquad \varphi(F,\zeta) = |F-\zeta| - F_y \tag{6}$$

We note that the following important relationship holds:

$$\frac{1}{k_0} + \frac{1}{k_h} = \frac{1}{k_1} \tag{7}$$

Yield functions accounting for biaxial shear interaction are presented in a later section.

2.2 Low friction sliding bearings

The behavior of the LFSBs is defined by extending to two dimensions the Coulomb friction model shown in Fig. 2. We note that a finite, albeit large, initial stiffness, k_{0c}, is introduced in the friction model. Such a stiffness is large enough so as not to change the physical behavior of the sliding isolators and it guarantees strict convexity of the optimization problem stated in a following section. For the sliding isolators, the following form of complementary stored energy and dissipation functions are used:

$$\psi^c(\mathbf{F}_i) = \frac{1}{2}\mathbf{F}_i^T\mathbf{A}_{Si}\mathbf{F}_i \qquad \phi^c(\mathbf{F}_i) = \chi_E(\mathbf{F}_i) \tag{8}$$

where $\mathbf{A}_{Si} = \mathrm{diag}(1/k_{0c}, 1/k_{0c})$, and χ_E is in this case the indicator function of the convex set:

$$E = \left\{ (\mathbf{F}_i) \middle| \varphi(\mathbf{F}_i) < 0 \right\} \tag{9}$$

When one-dimensional ideal plastic behavior is considered, as shown in Fig. 2, we have:

$$\psi^c(F) = \frac{1}{2}\frac{F^2}{k_{0c}} \qquad \varphi(F) = |F| - F_c \tag{10}$$

3 Proposed convex optimization procedure

In this section, the equations governing the behavior of a hybrid base isolation system composed of HDRBs and LFSBs are presented. Time discretization and manipulation of these equations is shown to lead to the formulation of a convex optimization problem for the incremental state update.

3.1 Governing equations

The governing equations of a spatially discretized HBIS model can be obtained as the Euler–Lagrange equations of a generalized Hamilton's principle [30] and written as

$$\begin{aligned} &\mathbf{M}\dot{\mathbf{v}}_0 + \mathbf{C}\mathbf{v}_\mathbf{0} + \mathbf{H}^T\mathbf{F} = \mathbf{P} \\ &\frac{d}{dt}\left(\partial_\mathbf{F}\psi^c(\mathbf{F},\boldsymbol{\zeta})\right) + \partial_\mathbf{F}\phi^c(\mathbf{F},\boldsymbol{\zeta}) - \mathbf{H}\mathbf{v}_0 = \mathbf{0} \\ &\frac{d}{dt}\left(\partial_\zeta\psi^c(\mathbf{F},\boldsymbol{\zeta})\right) + \partial_\zeta\phi^c(\mathbf{F},\boldsymbol{\zeta}) = \mathbf{0} \end{aligned} \tag{11}$$

The first of Eq. (11), already presented in Sect. 2, is the classic equation of motion expressing momentum conservation, the second expresses compatibility of deformation in the isolators and the third represents the evolution of the constitutive internal variables. $\boldsymbol{\zeta} \in \mathbb{R}^{N_r}$ is the vector of conjugates of the plastic strains in the HDRBs, N_r being the number of HDRBs in the system. When specialized to the complementary stored energy, ψ^c, given in Eqs. (2) and $(8)_1$, (11) may be written as

$$\begin{aligned} &\mathbf{M}\dot{\mathbf{v}}_0 + \mathbf{C}\mathbf{v}_\mathbf{0} + \mathbf{H}^T\mathbf{F} = \mathbf{P} \\ &\mathbf{A}\dot{\mathbf{F}} + \partial_\mathbf{F}\phi^c(\mathbf{F},\boldsymbol{\zeta}) - \mathbf{H}\mathbf{v}_0 = \mathbf{0} \\ &\mathbf{A}_h\dot{\boldsymbol{\zeta}} + \partial_\zeta\phi^c(\mathbf{F},\boldsymbol{\zeta}) = \mathbf{0} \end{aligned} \tag{12}$$

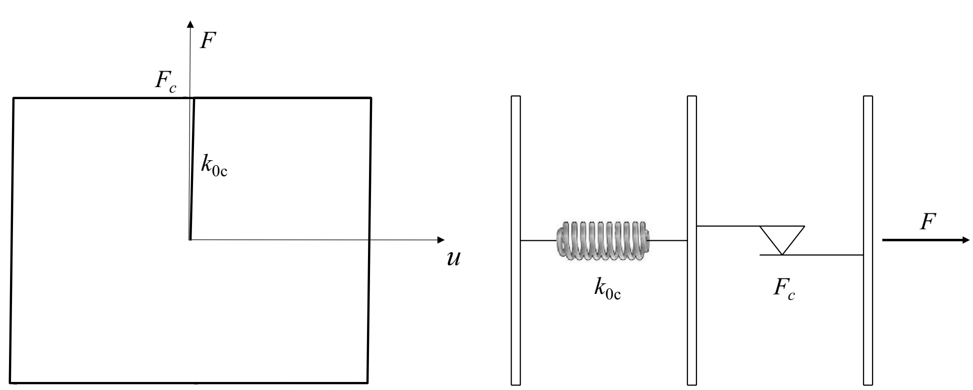

Fig. 2 Constitutive model for LFSBs

where $\mathbf{A} \in \mathbb{R}^{2N\times 2N}$ is the diagonal matrix of elastic compliances in all the isolators, and $\mathbf{A}_h \in \mathbb{R}^{2N_r\times 2N_r}$ is the diagonal matrix of compliances related to hardening in the HDRBs. In the next section, the governing equations are discretized in time leading to the formulation of a convex minimization problem.

3.2 Time discretization and optimization problem

Following [22], Eq. (12) are discretized in time using central differences and the midpoint rule. We note that in the case of linear elasticity this choice of discretization leads to Newmark's integration method with constant average acceleration [30]. Discretizing the first of Eq. (12) gives:

$$\mathbf{M}\left(\frac{\mathbf{v}_0^{n+1} - \mathbf{v}_0^n}{\Delta t}\right) + \mathbf{C}\left(\frac{\mathbf{v}_0^{n+1} + \mathbf{v}_0^n}{2}\right) + \mathbf{H}^T\left(\frac{\mathbf{F}^{n+1} + \mathbf{F}^n}{2}\right) = \frac{\mathbf{P}^{n+1} + \mathbf{P}^n}{2} \tag{13}$$

where Δt is the time increment and superscripts denote discrete times. Equation (13) may then be rearranged leading to:

$$\mathbf{v}_0^{n+1} = \bar{\mathbf{M}}^{-1}\left(\mathbf{b}_1 - \frac{\Delta t}{2}\mathbf{H}^T\mathbf{F}^{n+1}\right) \tag{14}$$

where $\bar{\mathbf{M}} = \mathbf{M} + \frac{\Delta t}{2}\mathbf{C}$ and:

$$\mathbf{b}_1 = \left(\mathbf{M} - \frac{\Delta t}{2}\mathbf{C}\right)\mathbf{v}_0^n + \frac{\Delta t}{2}\left(\mathbf{P}^{n+1} + \mathbf{P}^n\right) - \frac{\Delta t}{2}\mathbf{H}^T\mathbf{F}^n \tag{15}$$

We now discretize the second of Eqs. (12), which after rearranging and substituting Eq. (14) for $\mathbf{v}_0^{n+1}$ gives:

$$\left(\mathbf{A} + \frac{\Delta t^2}{4}\mathbf{H}\bar{\mathbf{M}}^{-1}\mathbf{H}^T\right)\mathbf{F}^{n+1} + \frac{\Delta t}{2}\partial_{\mathbf{F}}\phi^c\left(\mathbf{F}^{n+1}, \zeta^{n+1}\right) = \mathbf{b}_2 \tag{16}$$

where

$$\mathbf{b}_2 = \mathbf{A}\mathbf{F}^n + \frac{\Delta t}{2}\mathbf{H}\bar{\mathbf{M}}^{-1}\mathbf{b}_1 + \frac{\Delta t}{2}\mathbf{H}\mathbf{v}_0^n - \frac{\Delta t}{2}\partial_{\mathbf{F}}\phi^c(\mathbf{F}^n, \zeta^n) \tag{17}$$

Finally, by discretizing the third of Eqs. (12) we get:

$$\mathbf{A}_h\zeta^{n+1} + \frac{\Delta t}{2}\partial_\zeta\phi^c\left(\mathbf{F}^{n+1}, \zeta^{n+1}\right) = \mathbf{b}_3 \tag{18}$$

where

$$\mathbf{b}_3 = \mathbf{A}_h\zeta^n - \frac{\Delta t}{2}\partial_\zeta\phi^c(\mathbf{F}^n, \zeta^n) \tag{19}$$

It is easy to recognize nonlinear Eqs. (16) and (18) as the first-order necessary optimality conditions of the following minimization problem:

$$\begin{aligned}\min_{\mathbf{F},\zeta}\ & \frac{1}{2}\mathbf{F}^T\left(\mathbf{A} + \frac{\Delta t^2}{4}\mathbf{H}\bar{\mathbf{M}}^{-1}\mathbf{H}^T\right)\mathbf{F} \\ & + \frac{1}{2}\zeta^T\mathbf{A}_h\zeta + \frac{\Delta t}{2}\phi^c(\mathbf{F}, \zeta) - \mathbf{b}_2^T\mathbf{F} - \mathbf{b}_3^T\zeta\end{aligned} \tag{20}$$

Given that the complementary stored energy and dissipation functions are convex, and that matrix $\bar{\mathbf{M}}$ is positive definite, (20) represents a convex minimization problem and, as such, the first-order optimality conditions are also sufficient for the solution to be a global minimum. Since the dissipation potential, ϕ^c, is represented by indicator functions of the elastic region of the isolators, minimization problem (20) may be restated as:

$$\begin{aligned}\min_{\mathbf{F},\zeta}\ & \frac{1}{2}\mathbf{F}^T\left(\mathbf{A} + \frac{\Delta t^2}{4}\mathbf{H}\bar{\mathbf{M}}^{-1}\mathbf{H}^T\right)\mathbf{F} + \frac{1}{2}\zeta^T\mathbf{A}_h\zeta - \mathbf{b}_2^T\mathbf{F} - \mathbf{b}_3^T\zeta \\ \text{subject to}\ & \varphi(\mathbf{F}, \zeta) \le 0\end{aligned} \tag{21}$$

where the yield functions, φ, of the isolators appear as inequality constraints and the corresponding Lagrange multipliers are the incremental plastic strains. The constraints represent the convex elastic region and, therefore, (21) is an inequality constrained convex minimization problem. Several strategies and algorithms exist for the solution of this kind of convex quadratic programming problems [17, 18]. Particularly appealing are *interior-point* methods as they are relatively easy to implement and quite efficient on certain types of problems. They were first developed for large linear programming problems in the 1980s and quickly became strong competitors of the simplex method. Another important class of methods for constrained minimization attempt to solve the original constrained problem through a sequence of unconstrained subproblems. These are the *penalty*, *barrier* and *augmented Lagrangian* methods. A minimization algorithm based on an *augmented Lagrangian* approach [17] and Newton's method was developed for collapse simulations of large-scale structures by Sivaselvan et al. [22].

Conventional displacement-based approaches such as Newton's method based on the tangent stiffness matrix require some sort of iteration procedure that is not always guaranteed to converge. On the other hand, one advantage of relying on convex optimization procedures combined with interior point algorithms is that convergence is theoretically guaranteed [19]. Moreover, Sivaselvan et al. [22] have shown that the computational effort required for convergence of the minimization procedure does not increase significantly, even with a considerable increase of the time increment. As a first step, in this paper we discuss the use of readily available MATLAB [31] minimization functions *quadprog* and *fmincon* for the solution of (21). The former solves convex quadratic programming problems with linear inequality constraints using a predictor–corrector *interior-point* algorithm proposed by Mehrotra [32]. The latter minimizes nonlinear functions subjected to nonlinear inequality constraints using an *interior-point* algorithm based on the *logarithmic barrier* method [33–35].

3.3 Yield functions and constraints

The purpose of this subsection is to show how different interaction diagrams can be considered using the proposed formulation and how these can be implemented using Matlab functions *quadprog* and *fmincon* [31]. Minimization function *quadprog* can be used when the interaction diagrams may be approximated by convex polygons, while function *fmincon* must be used when considering convex nonlinear interaction domains. When using functions *quadprog* and *fmincon*, we set the optimization problem (21) in the following form:

$$\min_{\mathbf{x}} \; \frac{1}{2}\mathbf{x}^T\mathbf{Q}\mathbf{x} + \mathbf{f}^T\mathbf{x}$$
$$\text{subject to} \quad \begin{cases} \mathbf{A}_{in}\mathbf{x} \le \mathbf{b} & \text{linear constraints (quadprog)} \\ \mathbf{c}(\mathbf{x}) \le \mathbf{0} & \text{nonlinear constraints (fmincon)} \end{cases} \tag{22}$$

where

$$\mathbf{x} = \begin{bmatrix} \mathbf{F} \\ \zeta \end{bmatrix} \quad \mathbf{Q} = \begin{bmatrix} \mathbf{A} + \frac{\Delta t^2}{4}\mathbf{H}\bar{\mathbf{M}}^{-1}\mathbf{H}^T & \mathbf{0} \\ \mathbf{0} & \mathbf{A}_h \end{bmatrix} \quad \mathbf{f} = \begin{bmatrix} -\mathbf{b}_1 \\ -\mathbf{b}_2 \end{bmatrix} \tag{23}$$

The linear and nonlinear constraints in (22) represent the yield functions for the isolators. Different forms of biaxial shear interaction may be considered such as those plotted in Fig. 3. The square diagram (a) assumes no interaction whereas a more realistic shear interaction diagram for circular seismic isolation bearings is given by (d). Diagrams (b) and (c) are represented to illustrate how by increasing its number of sides, a polygon interaction diagram may be used to approximate the actual circular one. For large scale problems, it could be convenient to select the algorithm to be used based on a tradeoff between accuracy and computational cost.

The constraint inequalities related to biaxial shearing of a single rubber isolator are given below. For the sake of illustration, biaxial shear interaction diagrams (b) and (d) of Fig. 3 are considered. In the first case, the constraints are linear and given by:

$$\begin{aligned} &F_1 - \zeta_1 + F_2 - \zeta_2 \le F_y && -F_1 + \zeta_1 + F_2 - \zeta_2 \le F_y \\ &-F_1 + \zeta_1 - F_2 + \zeta_2 \le F_y && F_1 - \zeta_1 - F_2 + \zeta_2 \le F_y \end{aligned} \tag{24}$$

These constraints can be written in the form (22) by setting:

$$\mathbf{A}_{in} = \begin{bmatrix} 1 & 1 & -1 & -1 \\ -1 & 1 & 1 & -1 \\ -1 & -1 & 1 & 1 \\ 1 & -1 & -1 & 1 \end{bmatrix} \quad \mathbf{x} = \begin{bmatrix} F_1 \\ F_2 \\ \zeta_1 \\ \zeta_2 \end{bmatrix} \quad \mathbf{b} = F_y \begin{bmatrix} 1 \\ 1 \\ 1 \\ 1 \end{bmatrix} \tag{25}$$

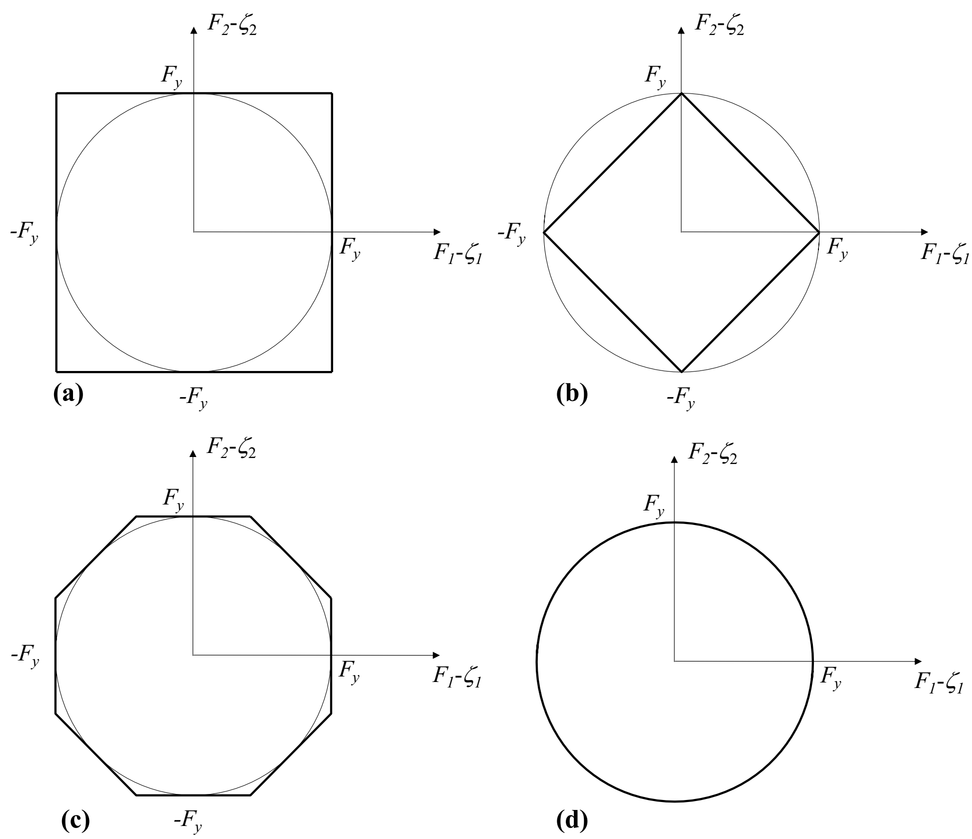

Fig. 3 Bidirectional shear force interaction diagrams

In the second case, the one quadratic constraint is given by:

$$c(F_1, F_2, \zeta_1, \zeta_2) = (F_1 - \zeta_1)^2 + (F_2 - \zeta_2)^2 - F_y^2 \leq 0 \quad (26)$$

3.4 Proposed algorithm

The algorithm used for implementation of the proposed procedure is summarized in Procedure 1. In Sect. 4, numerical examples are presented, to illustrate the working of the numerical algorithm.

3.5 Static displacement-controlled simulations

In the case of static displacement-controlled simulations as those presented in Sect. 4.2, the system of governing Eq. (12) may be reduced to:

$$\begin{aligned} &\mathbf{A}\dot{\mathbf{F}} + \partial_{\mathbf{F}}\phi^c(\mathbf{F}, \boldsymbol{\zeta}) - \dot{\mathbf{u}} = \mathbf{0} \\ &\mathbf{A}_h\dot{\boldsymbol{\zeta}} + \partial_{\zeta}\phi^c(\mathbf{F}, \boldsymbol{\zeta}) = \mathbf{0} \end{aligned} \quad (27)$$

where $\mathbf{F} = (F_1,\ F_2)^T$, $\mathbf{u} = (u_1,\ u_2)^T$, $\mathbf{A} = \mathrm{diag}(1/k_0,\ 1/k_0)$, $\mathbf{A}_h = \mathrm{diag}(1/k_h,\ 1/k_h)$. Discretizing Eqs. (27) in time using Backward–Euler gives:

$$\begin{aligned} &\mathbf{A}\frac{\mathbf{F}^{n+1} - \mathbf{F}^n}{\Delta t} + \partial_{\mathbf{F}}\phi^c(\mathbf{F}^{n+1}, \boldsymbol{\zeta}^{n+1}) - \frac{(\mathbf{u}^{n+1} - \mathbf{u}^n)}{\Delta t} = \mathbf{0} \\ &\mathbf{A}_h\frac{\boldsymbol{\zeta}^{n+1} - \boldsymbol{\zeta}^n}{\Delta t} + \partial_{\zeta}\phi^c(\mathbf{F}^{n+1}, \boldsymbol{\zeta}^{n+1}) = \mathbf{0} \end{aligned} \quad (28)$$

Equations (28) can be rearranged and written as:

$$\begin{aligned} &\mathbf{A}\mathbf{F}^{n+1} + \Delta t\partial_{\mathbf{F}}\phi^c(\mathbf{F}^{n+1}, \boldsymbol{\zeta}^{n+1}) = \mathbf{b}_2 \\ &\mathbf{A}_h\boldsymbol{\zeta}^{n+1} + \Delta t\partial_{\zeta}\phi^c(\mathbf{F}^{n+1}, \boldsymbol{\zeta}^{n+1}) = \mathbf{b}_3 \end{aligned} \quad (29)$$

where $\mathbf{b}_2 = \mathbf{A}\mathbf{F}^n + (\mathbf{u}^{n+1} - \mathbf{u}^n) = \mathbf{A}\mathbf{F}^n + \Delta\mathbf{u}_n$ and $\mathbf{b}_3 = \mathbf{A}_h\mathbf{F}^n$. It is easy to recognize nonlinear Eqs. (29) as the first-order necessary optimality conditions of the following minimization problem:

$$\min_{\mathbf{F},\zeta}\ \frac{1}{2}\mathbf{F}^T\mathbf{A}\mathbf{F} + \frac{1}{2}\boldsymbol{\zeta}^T\mathbf{A}_h\boldsymbol{\zeta} + \frac{\Delta t}{2}\phi^c(\mathbf{F}, \boldsymbol{\zeta}) - \mathbf{b}_2^T\mathbf{F} - \mathbf{b}_3^T\boldsymbol{\zeta} \quad (30)$$

Procedure 1 Time increment algorithm

1. *Initial calculations*

Form matrices $\mathbf{A}, \mathbf{A}_h, \mathbf{H}, \mathbf{M}, \mathbf{C}, \mathbf{P}$ (see Section 3.2)

Define constraint matrices $\mathbf{A}_{in}, \mathbf{b}, \mathbf{c}$ (see Section 3.4)

Select Δt

$$\bar{\mathbf{M}} = \mathbf{M} + \frac{\Delta t}{2}\mathbf{C}$$

$$\mathbf{Q} = \begin{bmatrix} \mathbf{A} + \frac{\Delta t^2}{4}\mathbf{H}\bar{\mathbf{M}}^{-1}\mathbf{H}^T & \mathbf{0} \\ \mathbf{0} & \mathbf{A}_h \end{bmatrix}$$

State determination: $\mathbf{v}_0^0, \mathbf{F}^0, \boldsymbol{\zeta}^0$

2. *Calculations for each time step*, $n = 0, 1, 2\ldots$ (see Sections 3.3 and 3.4)

$$\mathbf{b}_1 = \left(\mathbf{M} - \frac{\Delta t}{2}\mathbf{C}\right)\mathbf{v}_0^n + \frac{\Delta t}{2}(\mathbf{P}^{n+1} + \mathbf{P}^n) - \frac{\Delta t}{2}\mathbf{H}^T\mathbf{F}^n$$

$$\mathbf{b}_2 = \mathbf{A}\mathbf{F}^n + \frac{\Delta t}{2}\mathbf{H}\bar{\mathbf{M}}^{-1}\mathbf{b}_1 + \frac{\Delta t}{2}\mathbf{H}\mathbf{v}_0^n - \frac{\Delta t}{2}\partial_{\mathbf{F}}\phi^c(\mathbf{F}^n, \boldsymbol{\zeta}^n)$$

$$\mathbf{b}_3 = \mathbf{A}_h\boldsymbol{\zeta}^n - \frac{\Delta t}{2}\partial_{\zeta}\phi^c(\mathbf{F}^n, \boldsymbol{\zeta}^n)$$

$$\mathbf{f} = \begin{bmatrix} -\mathbf{b}_1 \\ -\mathbf{b}_2 \end{bmatrix}$$

$$\mathbf{x}^{n+1} = \begin{bmatrix} \mathbf{F}^{n+1} \\ \boldsymbol{\zeta}^{n+1} \end{bmatrix} = \mathrm{fmincon}(\mathbf{Q}, \mathbf{f}, \mathbf{x}^n, \mathbf{c}) \quad \text{or} \quad \mathbf{x}^{n+1} = \begin{bmatrix} \mathbf{F}^{n+1} \\ \boldsymbol{\zeta}^{n+1} \end{bmatrix} = \mathrm{quadprog}(\mathbf{Q}, \mathbf{f}, \mathbf{A}_{in}, \mathbf{b})$$

$$\mathbf{v}_0^{n+1} = \bar{\mathbf{M}}^{-1}\left(\mathbf{b}_1 - \frac{\Delta t}{2}\mathbf{H}^T\mathbf{F}^{n+1}\right)$$

$$\partial_{\mathbf{F}}\phi^c(\mathbf{F}^{n+1}, \boldsymbol{\zeta}^{n+1}) = \frac{2}{\Delta t}\left[\mathbf{b}_2 - \left(\mathbf{A} + \frac{\Delta t^2}{4}\mathbf{H}\mathbf{M}^{-1}\mathbf{H}^T\right)\mathbf{F}^{n+1}\right]$$

$$\partial_{\zeta}\phi^c(\mathbf{F}^{n+1}, \boldsymbol{\zeta}^{n+1}) = \frac{2}{\Delta t}(\mathbf{b}_3 - \mathbf{A}_h\boldsymbol{\zeta}^{n+1})$$

3. *Replace* n *by* $n+1$ *and implement calculations in step* 2 *for next time increment*

which can be restated as:

$$\min_{\mathbf{F},\boldsymbol{\zeta}} \; \frac{1}{2}\mathbf{F}^T\mathbf{A}\mathbf{F} + \frac{1}{2}\boldsymbol{\zeta}^T\mathbf{A}_h\boldsymbol{\zeta} - \mathbf{b}_2^T\mathbf{F} - \mathbf{b}_3^T\boldsymbol{\zeta} \quad \text{subject to} \quad \varphi(\mathbf{F},\boldsymbol{\zeta}) \le 0 \tag{31}$$

4 Numerical simulations

In this section, use of the proposed convex optimization procedure is illustrated through a series of numerical examples. The first example consists of subjecting one of the high damping rubber bearings of a real-world HBIS to bidirectional shearing under imposed displacement orbits; a second example concerns 2D dynamic analyses of the entire base isolation system subjected to earthquake motion.

4.1 Solarino base isolation system

At the turn of the century, a hybrid base isolation system composed of HDRBs and LFSBs was used for the seismic retrofit of two four-story reinforced concrete buildings in the town of Solarino in Sicily [36]. After the completion of the retrofitting works, one of the buildings was subjected to a set of free vibration tests by sudden release of a statically imposed initial displacement. Extensive structural identification studies [37–40] and earthquake response simulations [41, 42] were then conducted on the building using one-dimensional analytical and numerical models. In this work, these analyses are extended to the dynamic response of the Solarino base isolation system under two-dimensional excitation.

As shown in Fig. 4, the base isolation system of the Solarino buildings is composed of 12 HDRBs and 13 LFSBs. Figure 5 shows one isolator of each kind as they are mounted in the base isolation system.

We define a coordinate system with origin in the center of rigidity of the elastomeric bearings. The coordinates, x and y, of each isolator are given in Tables 1 and 2. As illustrated in Fig. 6, let $\mathbf{u}_0 = (u_{01}, u_{02}, \vartheta_0)^T$ be the vector of global degrees of freedom of the system. Assuming small rotations, the horizontal displacements, $\mathbf{u}_i = (u_{i1}, u_{i2})^T$, of generic isolator i may then be expressed as:

$$\mathbf{u}_i = \mathbf{H}_i\mathbf{u}_0 \tag{32}$$

where

$$\mathbf{H}_i = \begin{bmatrix} 1 & 0 & -y_i \\ 0 & 1 & x_i \end{bmatrix} \tag{33}$$

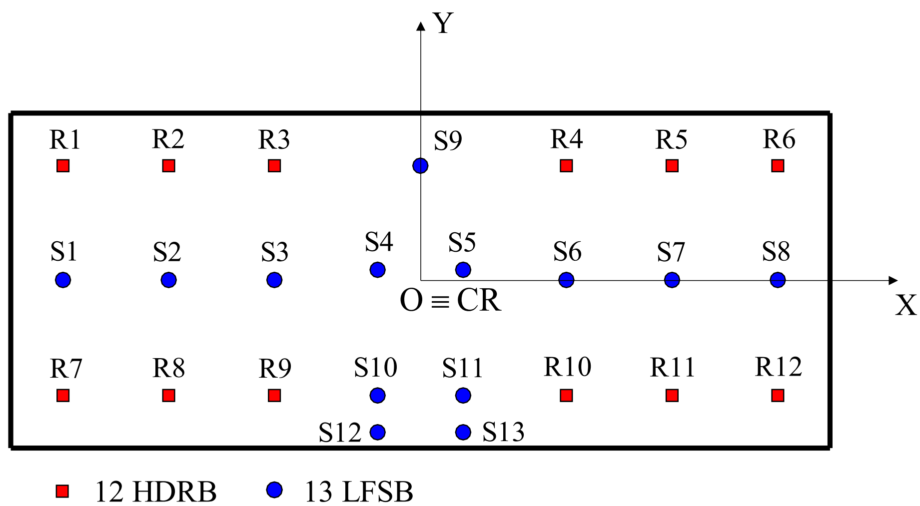

Fig. 4 Solarino hybrid base isolation system

Fig. 5 Bearings mounted in Solarino base isolation system: **a** HDRB, **b** LFSB

Table 1 Coordinates of HDRBs in Solarino base isolation system

ID	x (m)	y (m)	ID	x (m)	y (m)
R1	− 12.20	3.88	R7	− 12.20	− 3.88
R2	− 8.60	3.88	R8	− 8.60	− 3.88
R3	− 5	3.88	R9	− 5	− 3.88
R4	5	3.88	R10	5	− 3.88
R5	8.60	3.88	R11	8.60	− 3.88
R6	12.20	3.88	R12	12.20	− 3.88

Table 2 Coordinates of LFSBs in Solarino base isolation system

ID	x (m)	y (m)	ID	x (m)	y (m)
S1	− 12.20	0	S8	12.20	0
S2	− 8.60	0	S9	0	3.88
S3	− 5	0	S10	− 1.48	− 3.90
S4	− 1.48	0.38	S11	1.48	− 3.90
S5	1.48	0.38	S12	− 1.48	− 5.15
S6	5	0	S13	1.48	− 5.15
S7	8.6	0			

Owing to the static-kinematic duality established via the principle of virtual work, a similar expression relates the horizontal forces in isolator i, $\mathbf{F}_i = (F_{i1}, F_{i2})^T$, to forces in the global degrees of freedom, $\mathbf{F}_0 = (F_{01}, F_{02}, M_0)^T$, that is

$$\mathbf{H}_i^T \mathbf{F}_i = \mathbf{F}_0 \tag{34}$$

4.1.1 Modeling rubber isolator properties

The mechanical properties of the HDRBs were obtained by fitting a bilinear model to unidirectional shear force–deformation data obtained from displacement controlled harmonic tests performed at the University of Basilicata as part of the DPC-ReLUIS 2014 project [43]. The isolator tested has the following characteristics: total height 169 mm, diameter 500 mm, rubber height (t_r) 8×12 mm = 96 mm, steel height 3×11 mm = 33 mm, end plates 2×20 mm = 40 mm. Several tests were performed with a frequency of 0.5 Hz and maximum shear deformation, $\gamma_{max} = u_{max}/t_r$, varying between 5 and 200%. As shown in Fig. 7, the parameters of the bilinear model used for the simulations were calibrated using the measured cyclic force–deformation curve at $\gamma_{max} = 160\%$. The identified parameters are: initial elastic stiffness, $k_0 = 3674.10$ kN/m; post-elastic stiffness, $k_1 = 739.68$ kN/m; yield strength $F_y = 27.87$ kN.

4.1.2 Modeling sliding isolator properties

The dynamic coefficient of friction, μ, for the LFSBs, determined from previous identification studies [2] of the Solarino base isolation system, was taken equal to 0.75%. The Coulomb friction force, $F_c = P$, on each isolator was then calculated based on its axial load, P, under the seismic mass of the building. These axial forces were computed via static analysis in SAP2000 [44] of a detailed finite element model of the building. For details of the building, the reader is referred to [45]. Axial loads and estimated friction forces on the sliding isolators are given in Table 3. The value used as the artificial initial stiffness for the Coulomb friction model is $k_{0c} = 1e6$ kN/m.

4.1.3 Mass matrix and effective earthquake forces

Due to mass eccentricity and small asymmetries in the distribution of the sliding bearings, the Solarino isolation system shown in Fig. 4 is not perfectly symmetric. The mass matrix is given by:

$$\mathbf{M} = \begin{bmatrix} m & 0 & -S_x \\ 0 & m & S_y \\ -S_x & S_y & I_0 \end{bmatrix} \tag{35}$$

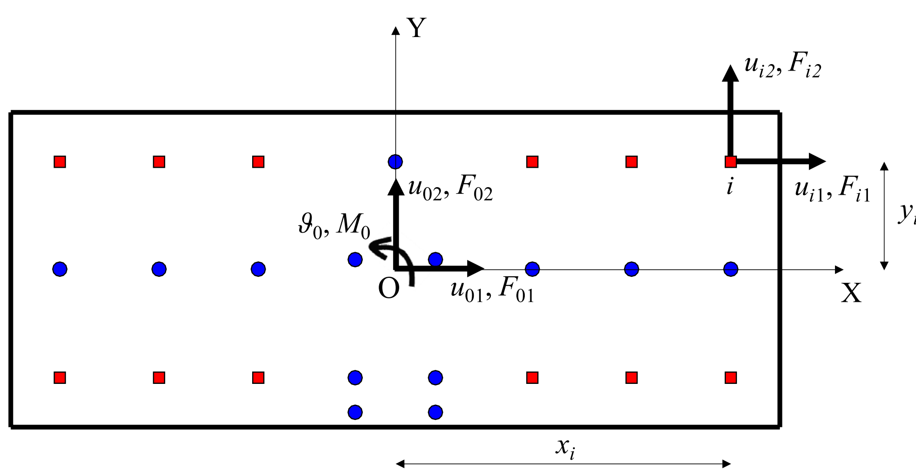

Fig. 6 Displacements and forces on generic isolator and at the global degrees of freedom

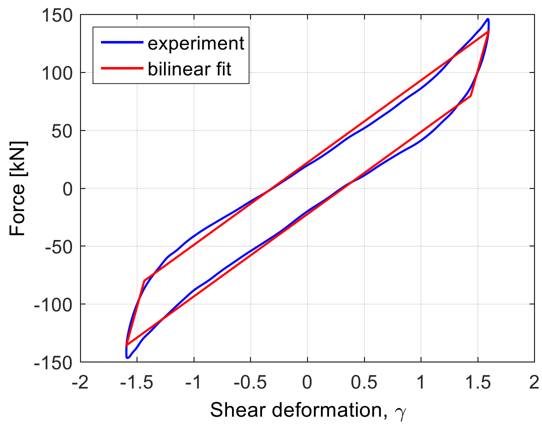

Fig. 7 Experimental and fitted force–deformation response of HDRB ($\gamma_{max}=160\%$)

Table 3 Axial loads, P, and friction forces, F_c, on LFSBs

ID	P (kN)	$F_c=\mu P$ (kN)	ID	P (kN)	$F_c=\mu P$ (kN)
S1	710	5.33	S8	715	5.36
S2	627	4.70	S9	753	5.65
S3	631	4.73	S10	516	3.87
S4	608	4.56	S11	528	3.96
S5	616	4.62	S12	235	1.76
S6	636	4.77	S13	243	1.82
S7	633	4.75			

Table 4 Mass properties and eccentricity

Mass of superstructure m	1500	kN s^2/m
Mass moment of inertia I_{cm}	1.29E+05	kN s^2 m
e_x	0.04	m
e_y	−0.13	m

where m is the total mass of the superstructure, $S_x=me_y$ and $S_y=me_x$ are the first moments of mass with respect to X and Y respectively, and $I_0=I_{cm}+m(e_x^2+e_y^2)$ is the mass moment of inertia about the vertical axis through the center of rigidity (subscript cm stands for center of mass). The position of the center of mass, along with the values of the total mass, m, and mass moment of inertia about the vertical axis through the center of mass, I_{cm}, were determined through a detailed finite element model of the building developed in SAP2000 and are given in Table 4. The effective earthquake forces are:

$$\mathbf{P}=-\mathbf{M}\boldsymbol{i}_x\ddot{u}_{gx}-\mathbf{M}\boldsymbol{i}_y\ddot{u}_{gy} \tag{36}$$

where $\ddot{u}_{gx}$ and $\ddot{u}_{gy}$ are the two orthogonal components of ground motion, EW and NS respectively, and the influence vectors, $\boldsymbol{i}_x=[1,\ 0,\ 0]^T$ and $\boldsymbol{i}_y=[0,\ 1,\ 0]^T$, represent the displacements of mass m resulting from static application of unit ground displacements, u_{gx} and u_{gy}.

4.2 Example 1: Bidirectional shearing of high damping rubber bearing

In this first example, one single rubber bearing of the Solarino base isolation system was subjected to the bidirectional displacement orbits shown in Fig. 8. Several simulations were conducted using the bidirectional shear interaction diagram of Fig. 3d.

The results in terms of biaxial resisting forces in the bearing are shown in Figs. 9 and 10 for different levels of maximum shear deformation, γ_{max}=50, 100 and 150%.

Coupling between components of motion is clear. The numerical simulations show that increasing the displacement in one direction while keeping the displacement in the orthogonal direction fixed (box orbit) affects the shear force in both directions. Moreover, due to interaction between components of motion, the shape of the loops at maximum strain is considerably changed (figure eight orbit)

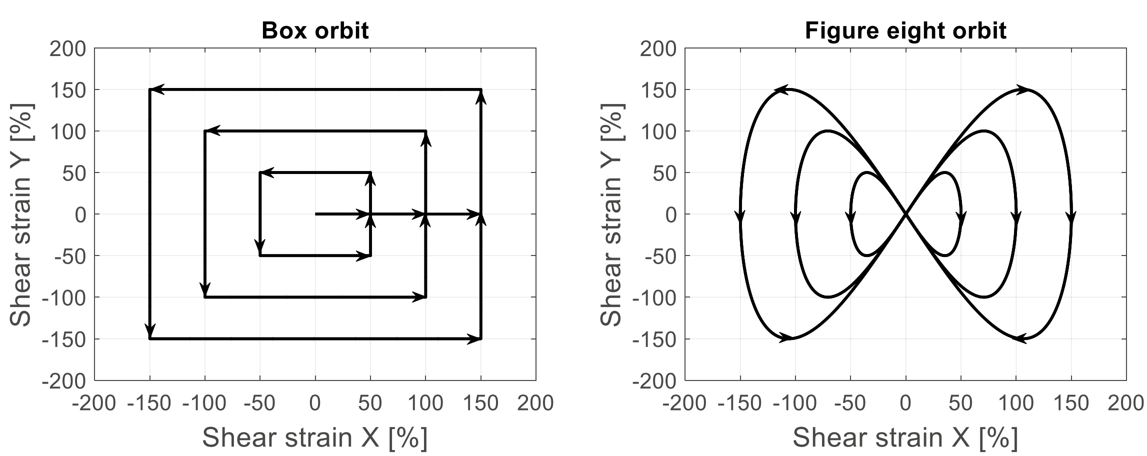

Fig. 8 Imposed displacement orbits

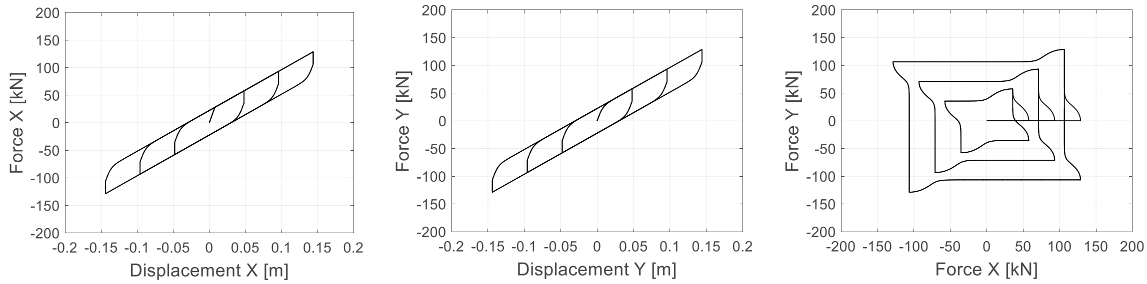

Fig. 9 Biaxial shear response of HDRB to box orbits

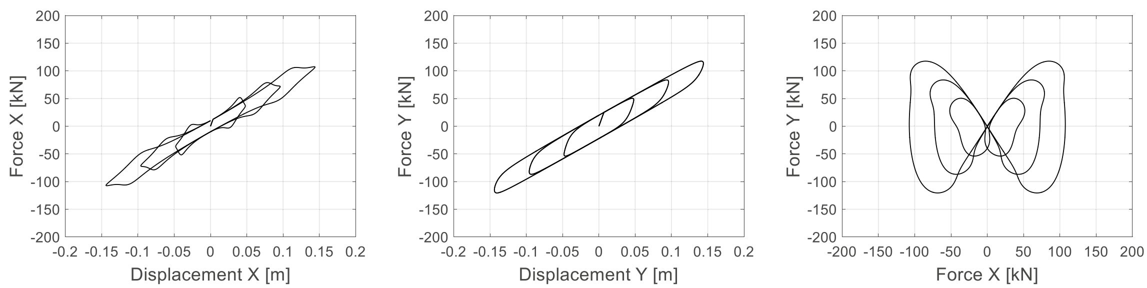

Fig. 10 Biaxial shear response of HDRB to figure eight orbits

Table 5 Characteristics and scaling factors of earthquakes selected for analysis (R is the minimum distance from the fault)

Earthquake	Station	R (km)	‖PGA‖ (g)	Scaling factor
L'Aquila 2009	AQK	4.8	0.388	0.78
Irpinia 1980	STR	4	0.330	0.31

as compared to those obtained under unidirectional loading (Fig. 7). The results of the simulations compare favorably, in a qualitative sense, to those obtained from bidirectional tests on similar bearings performed as part of the Caltrans Protective Systems Project at the University of California, Berkeley [3, 46–48]. Similar trends can also be seen in experiments by Abe et al. [12] and Yamamoto et al. [13].

4.3 Example 2: earthquake simulations

In a second numerical example, the Solarino base isolation system was subjected to bidirectional earthquake records scaled so that the 5% damped spectral acceleration of the EW component at the fundamental period of the base-isolated building ($T = 2.35$ s) be equal to that of the design spectrum provided by the seismic regulations at the time of the retrofit [49]. Two Italian acceleration records were considered, one from the L'Aquila 2009 event and another from the Irpinia 1980 earthquake. Characteristics and scaling factors of the ground motions are provided in Table 5. Design spectrum and response spectra of the scaled records are given in Fig. 11.

4.3.1 Response of the Solarino base isolation system

The simulations were carried out using the interaction diagram of Fig. 3d. The maximum displacements of the bearings were 19.64 cm under the AQK earthquake and 6.61 cm under the STR earthquake. These, both smaller than the maximum permissible displacement of 20 cm specified by the manufacturer, were exhibited by corner bearings, R1 and R12, respectively. We emphasize that the purpose of the simulations was not to assess the performance of the Solarino base isolation system but to illustrate the ability of the proposed formulation to compute the response of the base isolation system under bidirectional earthquake excitation. The bidirectional earthquake response of bearings R1 and R12 is shown in Figs. 12 and 13. Satisfaction of the plastic constraints during the simulations is illustrated in Fig. 14.

5 Concluding remarks

A formulation has been derived for the dynamic analysis of base isolation systems under bidirectional excitation. The force-based approach consists of casting the computation at each time step as a convex minimization problem. Coupling between the two horizontal components of response in the isolators is considered through bidirectional shear

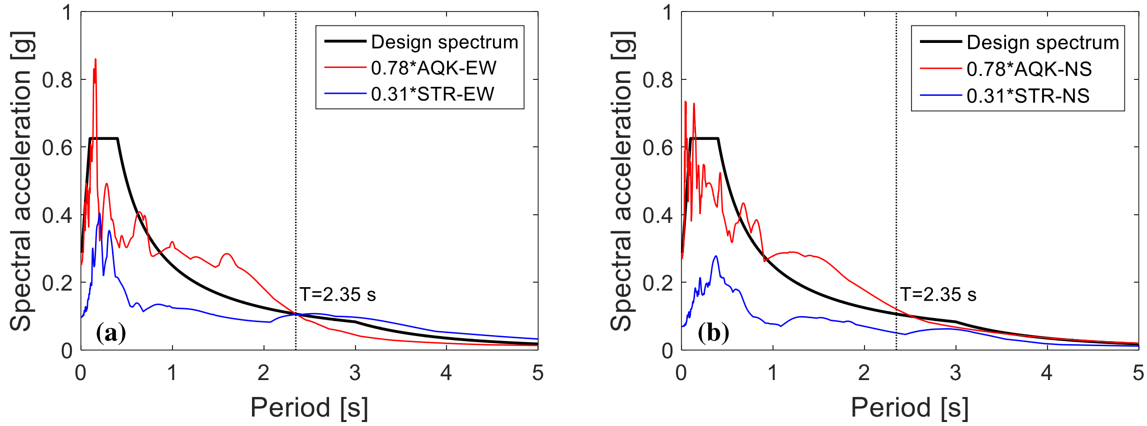

Fig. 11 Design spectrum and response spectra of bidirectional ground motions considered: **a** EW components, **b** NS components

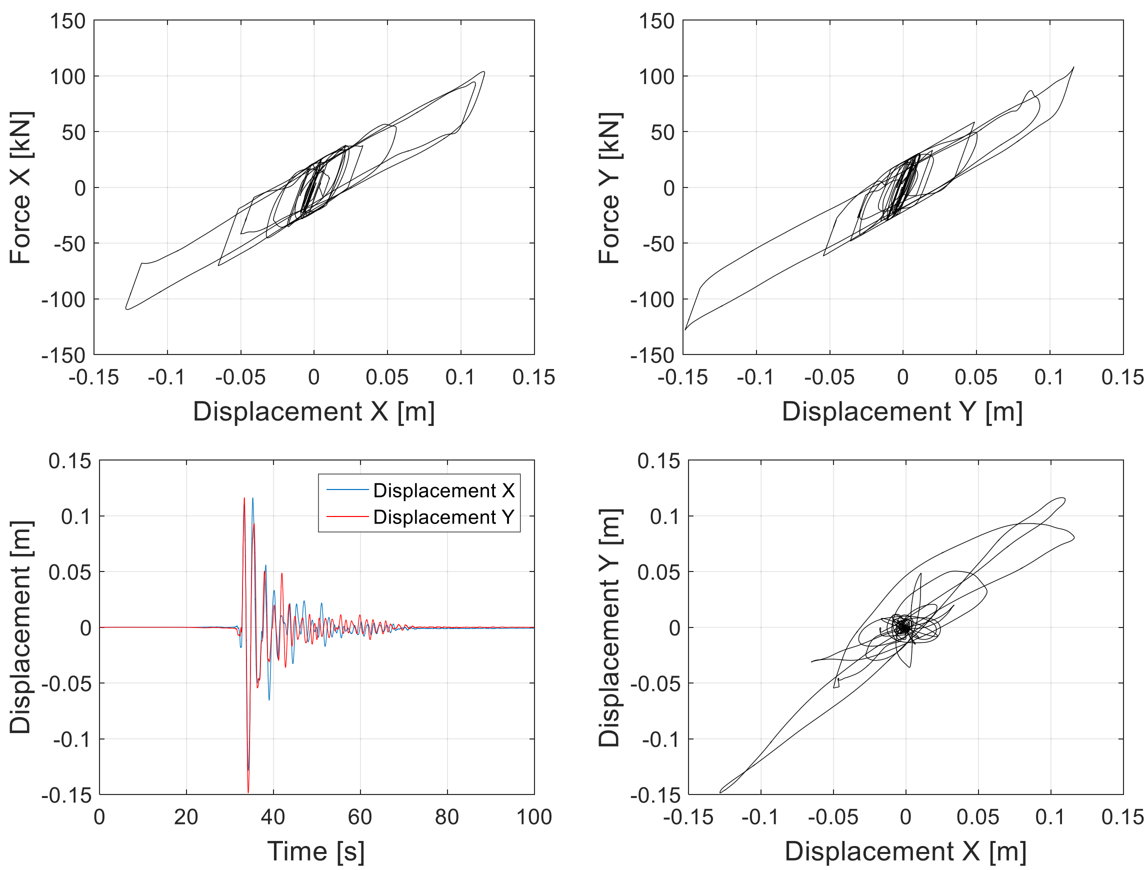

Fig. 12 Response of HDRB R1 to bidirectional AQK earthquake record

force interaction diagrams representing the constraints of the optimization problem. Numerical examples have been carried out to illustrate the approach and to simulate the response of the Solarino hybrid base isolation system to bidirectional ground motions. The proposed formulation can be easily applied to any base isolation system made with isolation devices whose unidirectional shear behavior can be approximated using bilinear models. Inclusion in the current framework of more complex hysteretic models [9, 11], as well as the effects of vertical loading on the bearings and coupling of vertical and horizontal motion, are the subject of ongoing work.

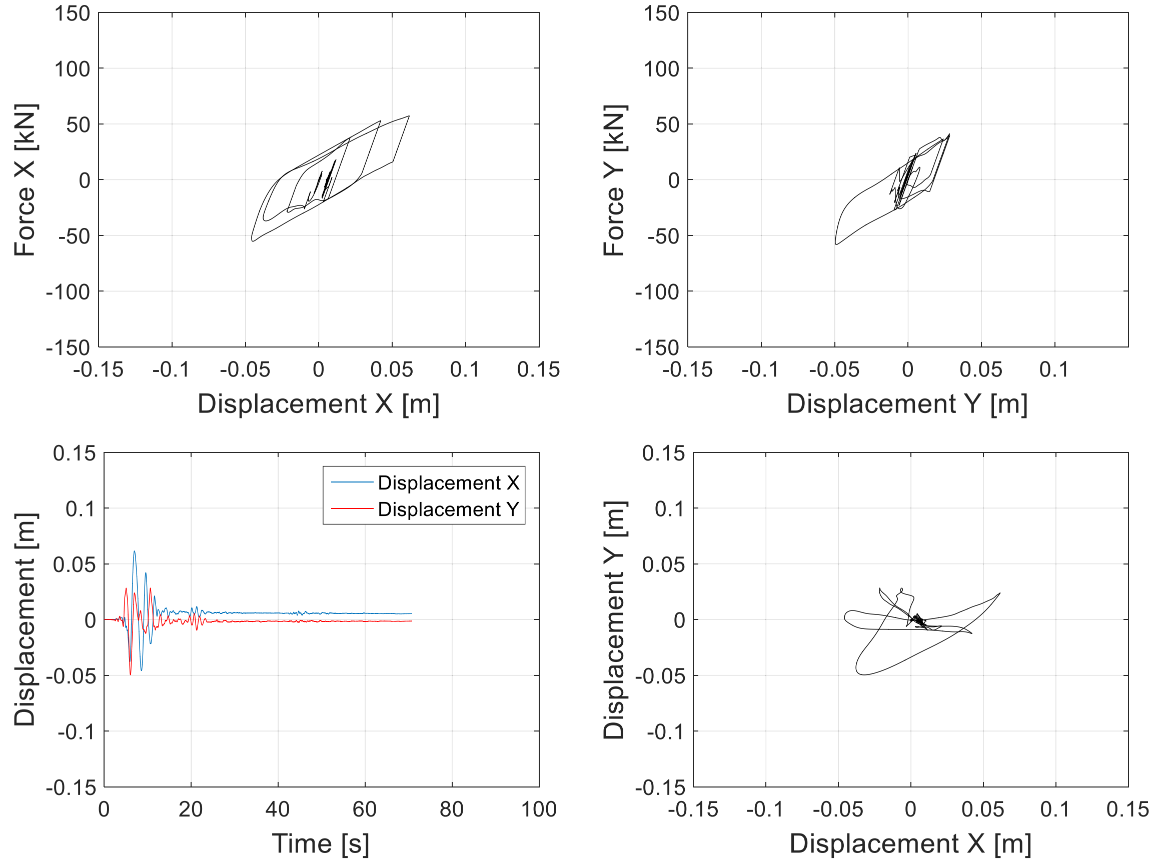

Fig. 13 Response of HDRB R12 to bidirectional STR earthquake record

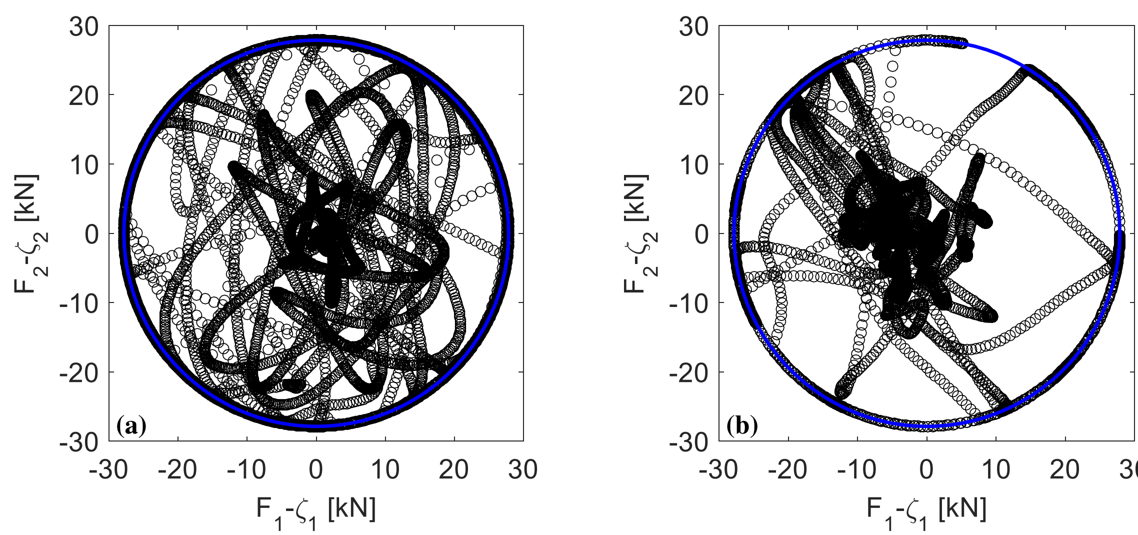

Fig. 14 Shear interaction diagram and plastic constraint satisfaction: **a** response of HDRB R1 to bidirectional AQK earthquake record, **b** response of HDRB R12 to bidirectional STR earthquake record

Acknowledgements The authors gratefully acknowledge financial support by ReLUIS (Italian National Network of University Earthquake Engineering Laboratories), 'Project D.P.C-ReLUIS 2014–2018'.

Compliance with ethical standards

Conflict of interest All authors have read and approved submission of the manuscript. The manuscript has not been published nor is it being considered for publication by other journals. The authors declare that they have no conflict of interest.

References

1. Markou AA, Oliveto ND, Athanasiou A (2017) Modelling of high damping rubber bearings. In: Sextos A, Manolis G (eds) Dynamic response of infrastructures to environmentally induced loads. Lecture notes in civil engineering, vol 2. Springer, Cham
2. Calvi PM, Calvi GM (2018) Historical development of friction-based seismic isolation systems. Soil Dyn Earthq Eng 106:14–30
3. Grant DN, Fenves GL, Whittaker AS (2004) Bidirectional modeling of high-damping rubber bearings. J Earthq Eng 8(S1):161–185
4. Park YJ, Wen YK, Ang AHS (1986) Random vibration of hysteretic systems under bi-directional ground motions. Earthq Eng Struct Dyn 14:543–557
5. Kumar M, Whittaker AS, Constantinou MC (2014) An advanced numerical model of elastomeric seismic isolation bearings. Earthq Eng Struct Dyn 43(13):1955–1974
6. Oliveto ND, Markou AA, Athanasiou A (2019) Modeling of high damping rubber bearings under bidirectional shear loading. Soil Dyn Earthq Eng 118:179–190
7. Bouc R (1971) Modele mathematique d'hysteresis. Acustica 24:16–25
8. Wen Y (1976) Method for random vibration of hysteretic systems. J Eng Mech Div ASCE 102(2):249–263
9. Hwang J, Wu J, Pan TC, Yang G (2002) A mathematical hysteretic model for elastomeric isolation bearings. Earthq Eng Struct Dyn 31(4):771–789
10. Vaiana N, Sessa S, Marmo F, Rosati L (2018) A class of uniaxial phenomenological models for simulating hysteretic phenomena in rate-independent mechanical systems and materials. Nonlinear Dyn 93(3):1647–1669
11. Vaiana N, Sessa S, Marmo F, Rosati L (2019) An accurate and computationally efficient uniaxial phenomenological model for steel and fiber reinforced elastomeric bearings. Compos Struct 211:196–212
12. Abe M, Yoshida J, Fujino Y (2004) Multiaxial behaviors of laminated rubber bearings and their modeling. I: experimental study. J Struct Eng 130:1119–1132
13. Yamamoto M, Minewaki S, Yoneda H, Higashino M (2012) Nonlinear behavior of high-damping rubber bearings under horizontal bidirectional loading: full-scale tests and analytical modeling. Earthq Eng Struct Dyn 41:1845–1860
14. Chopra AK (2012) Dynamics of structures: theory and applications to earthquake engineering. Prentice Hall, New Jersey
15. Nagarajaiah S, Reinhorn AM, Constantinou MC (1991) Nonlinear dynamic analysis of 3-D base-isolated structures. J Struct Eng ASCE 117(7):2035–2054
16. Greco F, Luciano R, Serino G, Vaiana N (2018) A mixed explicit-implicit time integration approach for nonlinear analysis of base-isolated structures. Ann Solid Struct Mech 10(1–2):17–29
17. Boyd SP, Vandenberghe L (2004) Convex optimization. Cambridge University Press, Cambridge
18. Nocedal J, Wright SJ (2006) Numerical optimization, 2nd edn. Springer, New York
19. Kanno Y (2011) Nonsmooth mechanics and convex optimization. CRC Press, Boca Raton
20. Cohn MZ, Maier G, Grierson DE (1979) Engineering plasticity by mathematical programming. In: Proceedings of the NATO Advanced Study Institute, University of Waterloo, Waterloo, Canada, 2–12 August 1977. Pergamon Press. New York
21. Maier GA (1970) Matrix structural theory of piecewise linear elastoplasticity with interacting yield planes. Meccanica 5(1):54
22. Sivaselvan MV, Lavan O, Dargush GF, Kurino H, Hyodo Y, Fukuda R, Sato K, Apostolakis G, Reinhorn AM (2009) Numerical collapse simulation of large-scale structural systems using an optimization-based algorithm. Earthq Eng Struct Dyn 38(5):655–677
23. Sivaselvan MV (2011) Complementarity framework for non-linear dynamic analysis of skeletal structures with softening hinges. Int J Numer Meth Eng 86:182–223
24. Oliveto ND, Sivaselvan MV (2011) Dynamic analysis of tensegrity structures using a complementarity framework. Comput Struct 89:2471–2483
25. Halphen B, Nguyen Quoc S (1975) Sur les materiaux standard generalises. Journal de Mecanique 14(1):39
26. Mielke A (2006) A mathematical framework for generalized standard materials in the rate-independent case. In: Multifield problems in solid and fluid mechanics. Springer, Berlin, pp 399–428
27. Architectural Institute of Japan (AIJ) (2016) Design recommendations for seismically isolated buildings. Committee for Seismically Isolated Structures, Japan
28. Rockafellar RT (1970) Convex analysis. Princeton University Press, Princeton
29. Hiriart-Urruty JB, Lemarechal C (1993) Convex analysis and minimization algorithms. Grundlehren der Mathematischen Wissenschaften. Springer, Berlin, pp 305–306
30. Sivaselvan MV, Reinhorn AM (2006) Lagrangian approach to structural collapse simulation. J Eng Mech (ASCE) 132(8):795–805
31. MATLAB Release (2011a) The MathWorks, Inc. Natick, MA, United States (2011)
32. Mehrotra S (1992) On the implementation of a primal-dual interior point method. SIAM J Optim 2:575–601
33. Byrd RH, Gilbert JC, Nocedal J (2000) A trust region method based on interior point techniques for nonlinear programming. Math Program 89(1):149–185
34. Byrd RH, Hribar ME, Nocedal J (1999) An interior point algorithm for large-scale nonlinear programming. SIAM J Optim 9(4):877–900
35. Waltz RA, Morales JL, Nocedal J, Orban D (2006) An interior algorithm for nonlinear optimization that combines line search and trust region steps. Math Program 107(3):391–408
36. Oliveto G, Granata M, Buda G, Sciacca P (2004) Preliminary results from full-scale free vibration tests on a four story reinforced concrete building after seismic rehabilitation by base isolation. In: JSSI 10th anniversary symposium on performance of response controlled buildings, Yokohama, Japan
37. Oliveto ND, Scalia G, Oliveto G (2008) Dynamic identification of structural systems with viscous and friction damping. J Sound Vib 318:911–926
38. Oliveto ND, Scalia G, Oliveto G (2010) Time domain identification of hybrid base isolation systems using free vibration tests. Earthq Eng Struct Dyn 39:1015–1038
39. Athanasiou A, De Felice M, Oliveto G, Oliveto PS (2011) Evolutionary algorithms for the identification of structural systems in earthquake engineering. In: Proceedings of International

Conference on Evolutionary Computation Theory and Applications (ECTA 11), France
40. Athanasiou A, De Felice M, Oliveto G, Oliveto PS (2013) Dynamical modeling and parameter identification of seismic isolation systems by evolution strategies. In: Studies in computational intelligence, vol 465. Springer, Berlin, pp 101–18
41. Oliveto G, Athanasiou A, Oliveto ND (2012) Analytical earthquake response of 1D hybrid base isolation systems. Soil Dyn Earthq Eng 43:1–15
42. Oliveto G, Oliveto ND, Athanasiou A (2014) Constrained optimization for 1-D dynamic and earthquake response analysis of hybrid base-isolation systems. Soil Dyn Earthq Eng 67:44–53
43. Markou AA, Oliveto G, Mossucca A, Ponzo FC (2014) Laboratory experimental tests on elastomeric bearings from the Solarino project. Task 1.1. report, WP1 Isolamento Sismico: Rapporto tecnico prove sperimentali progetto JETBIS e prove/analisi su isolatori elastomerici. DPC-ReLUIS project, pp 159–192
44. SAP2000. Computers and Structures, Inc. Walnut Creek, CA, United States
45. Oliveto G, Athanasiou A, Marino G, Granata M, Markou AA, Oliveto ND (2016) Adeguamento sismico degli edifici di Solarino. Prodotto finale del WP1: Progettazione di strutture sismicamente isolate. DPC-ReLUIS project, pp 15–77
46. Thompson ACT (1998) High damping rubber seismic isolation bearings—behavior and design implications. CE299 report, University of California, Berkeley
47. Morgan TA (2000) Characterization and seismic performance of high-damping rubber isolation bearings. CE299 report, University of California, Berkeley
48. Huang WH (2002) Bi-directional testing, modeling, and system response of seismically isolated bridges. Ph.D. Thesis, University of California, Berkeley
49. Presidenza del Consiglio Superiore dei Lavori Pubblici—Servizio Tecnico Centrale (1998) Linee Guida per Progettazione, Esecuzione e Collaudo di Strutture Isolate dal Sisma